RevMexAA (Serie de Conferencias), **36**, 163–170 (2009)

MAGNETOROTATIONAL INSTABILITY IN VISCOUS MEDIA: APPLICATION TO THE CENTRAL ENGINE OF GAMMA-RAY BURSTS

Y. Masada[1,2] and K. Shibata[2]

RESUMEN

En las regiones ultra densas y calientes de colapso de núcleos estelares, los neutrinos juegan un papel importamte en el transporte de energía y momento. Investigamos el crecimiento de la inestabilidad magnetorrotacional (MRI) en medios con viscosidad debida a neutrinos, usando cálculos lineales y no lineales. Del análisis linear local, encontramos que la viscosidad de neutrinos puede suprimir la MRI en el régimen de campos magnéticos débiles ($B \ll 10^{14}$G). Esto sugiere que la turbulencia MHD sostenida por la MRI no podría ser producida eficientemente en medios con viscosidad de neutrinos. Aplicando este resultado a un disco de "colapsar", que es una posible máquina central de los destellos de rayos gama (GRB), encontramos que la MRI puede suprimirse sólo en la parte central del disco. Basándonos en este resultado, proponemos un nuevo modelo de la evolución de un disco de "colapsar", el "disco de acreción episódico". Finalmente, presentamos nuestro reciente estudio numérico de la evolución no linear de la MRI en medios con viscosidad de neutrinos.

ABSTRACT

In ultra dense and hot regions realized in stellar core-collapse, neutrinos take a major role in the energy and momentum transports. We investigate the growth of the magnetorotational instability (MRI) in neutrino viscous media by using linear and nonlinear calculations. It is found from the local linear analysis that the neutrino viscosity can suppress the MRI in the regime of weak magnetic field ($B \ll 10^{14}$G). This suggests that MHD turbulence sustained by the MRI might not be driven efficiently in neutrino viscous media. Applying this result to a collapsar disk, which is known as the central engine of gamma-ray bursts (GRB), we find that the MRI can be suppressed only in its inner region. Based on this finding, a new evolutionary scenario of a collapsar disk, the "Episodic Disk Accretion Model" is proposed. Finally, we report our recent numerical study on the nonlinear evolution of the MRI in neutrino viscous media.

Key Words: accretion, accretion disks — black hole physics — gamma rays: bursts — instabilities — magnetic fields

1. INTRODUCTION

Gamma-ray bursts (GRBs) are the most energetic events in the universe. GRBs are generally considered to be powered by hyperaccretion onto a stellar-mass black hole, which is formed in the context of the "collapsar" scenario or merging scenario of compact objects (Narayan et al. 1992; Woosley 1993). The hyperaccretion rate is of the order of $0.1\ M_\odot\ \mathrm{s}^{-1}$ and the release of gravitational energy powers the burst.

A key process for releasing the gravitational energy of disk systems is the angular momentum transport. As in the case of the other disk systems, MHD turbulence sustained by magnetorotational instability (MRI) is believed to play an essential role in the angular momentum transport of the hyperaccretion disk of GRBs (Balbus & Hawley 1991; Lee et al. 2005). Physical conditions of the hyperaccretion disk are quite different from the ones of other disks. Because it is ultra-dense and hot like a supernova core, energy and momentum are mainly transported by the neutrinos in neutrino-opaque regions.

Masada et al. (2007a, hereafter MSS07) investigate the effect of neutrino transport on the MRI in the supernova core and show that the neutrino viscosity can suppress the MRI in the weakly magnetized case. The hyperaccretion disk is expected to have physical properties similar to the supernova core. The result of MSS07 can therefore be applied to hyperaccretion disks with only small modifications.

The growth time of the MRI in the absence of viscosity is given by λ/v_A, where λ is the wavelength of a perturbation and $v_A = B/(4\pi\rho)^{1/2}$ is the Alfvén speed. The MRI is suppressed dramatically if the growth time is longer than the viscous damping time $\sim \lambda^2/\nu$, where ν is the kinematic viscosity. There-

[1]Institute of Astronomy and Astrophysics, and Theoretical Institute for Advanced Research in Astrophysics (TIARA), Academia Sinica, Taipei 10617, Taiwan, R.O.C (masada@asiaa.sinica.edu.tw).

[2]Department of Astronomy, and Kwasan & Hida Observatories, Kyoto University, Kyoto 607-8471, Japan.

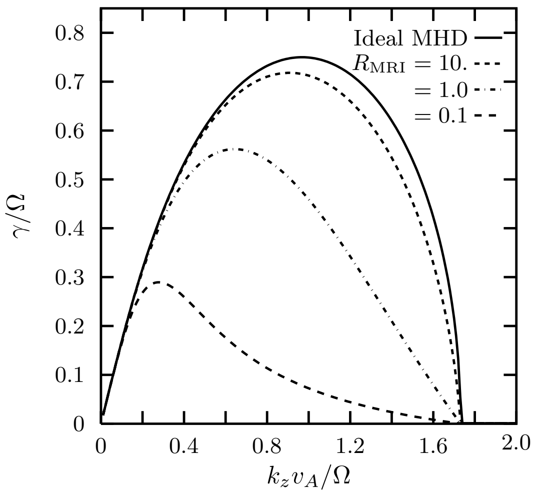

Fig. 1. The maximum growth rate of the MRI as a function of the wavenumber in cases with $R_{\rm MRI} = 0.1$, 1.0, 10.0 and ∞. A Keplerian rotation has been assumed ($q = -1.5$).

fore, a large enough viscosity can reduce the linear growth of the MRI. Since the typical wavelength of the MRI is $\lambda \sim v_A/\Omega$ with angular velocity Ω, the condition for an efficient growth of the MRI can be written as

$$R_{\rm MRI} \equiv LU/\nu = v_A^2/\nu\Omega \gtrsim 1\,, \qquad (1)$$

where $R_{\rm MRI}$ is the Reynolds number for MRI. We choose v_A/Ω as the typical length scale L and v_A as the velocity scale U. In the neutrino-opaque matter, the neutrino viscosity becomes quite large, so that the condition (1) would not be satisfied. We thus investigate where the MRI operates in the hyperaccretion disk, focusing on the neutrino viscous effect by using linear and nonlinear calculations.

2. LINEAR ANALYSIS

2.1. *Linear Dispersion Relation*

MSS07 derive the dispersion equation for the MRI including the effects of neutrino transport. We apply it to find the most unstable modes of the MRI in the hyperaccretion disk. A uniform vertical field is considered here. Considering only the damping effect of the neutrino viscosity, the dispersion equation in MSS07 can be written as

$$\tilde{\gamma}^4 + \frac{2}{R_{\rm MRI}}\tilde{k}^2\tilde{\gamma}^3 + \left[\frac{1}{R_{\rm MRI}^2}\tilde{k}^4 + 2\tilde{k}^2 + \left(\frac{\kappa}{\Omega}\right)^2\right]\tilde{\gamma}^2 + \frac{2}{R_{\rm MRI}}\tilde{k}^4\tilde{\gamma} + (\tilde{k}^4 - 2q\tilde{k}^2) = 0\,, \qquad (2)$$

where the $\tilde{\gamma} = \gamma/\Omega$ is the growth rate normalized by Ω, $\tilde{k} = k_z v_A/\Omega$ is the vertical wavenumber normalized by Ω/v_A, and $\kappa = 2(2+q)\Omega^2$ is the epicyclic frequency. The equation above is found to be characterized by the Reynolds number $R_{\rm MRI}$.

In order to show the general features of the dispersion equation (2), we solve it numerically and describe the linear growth rate of the MRI for the cases with $R_{\rm MRI} = 0.1$, 1.0, 10.0 and ∞ in Figure 1 (with $q = -1.5$ in all cases). We find that the upper limit of the unstable mode remains unchanged in spite of the size of $R_{\rm MRI}$ ($\tilde{k}_{\rm crit} = \sqrt{3}$). In contrast, the most unstable wavenumber decreases with $R_{\rm MRI}$. Figures 2a,b show the maximum growth rate and the most unstable wavenumber as a function of the Reynolds number. It is found from these figures that $\tilde{\gamma}$ and $\tilde{k}$ are proportional to $R_{\rm MRI}^{1/2}$ in the $R_{\rm MRI} \ll 1$ range.

The qualitative features of the most unstable mode are physically explained as follows: The viscous dissipation takes effect when the damping rate of a perturbation becomes comparable to the shear rate of the system, that is $k^2\nu \sim |{\rm d}\Omega/{\rm d}\ln r| \sim \Omega$. The most unstable wavenumber $k_{z,\rm max}$ therefore is

$$\tilde{k}_{z,\rm max} \simeq \left(v_A^2/\nu\Omega\right)^{1/2} = R_{\rm MRI}^{1/2}\,. \qquad (3)$$

Since the maximum growth rate of the MRI is typically equal to the Alfvén frequency of the fastest growing mode $\gamma_{\rm max} \simeq k_{z,\rm max}v_A$, it is given by

$$\gamma_{\rm max}/\Omega \simeq \left(v_A^2/\nu\Omega\right)^{1/2} = R_{\rm MRI}^{1/2}\,. \qquad (4)$$

It is interesting that the $R_{\rm MRI}$-dependence of the MRI is quite different from its dependence on the Lundquist number ($S_{\rm MRI} \equiv v_A^2/\eta\Omega$) in resistive media (Sano & Miyama 1999).

2.2. *Structure of the Hyperaccretion Disk*

2.2.1. *Neutrino Depth and Viscosity*

We need to know the amplitude of the neutrino viscosity and the neutrino depth in the hyperaccretion disk to investigate where the MRI operates. We treat, for simplicity, the neutrino transport with the diffusion approximation. The neutrino viscosity is assumed to be zero in the neutrino-transparent region. We consider that both absorption and scattering processes contribute to the neutrino depth and viscosity. The total neutrino depth $\tau_{\rm tot}$ is thus given by the sum of the absorptive and scattering neutrino depths,

$$\tau_{\rm tot} = \tau_{\rm abs} + \tau_{\rm sc} = 1.3 \times 10^{-38}T^2\rho H\,, \qquad (5)$$

(Di Matteo et al. 2002; Shapiro & Teukolsky 1983), where T is the temperature, ρ is the density, and H is the scale height.

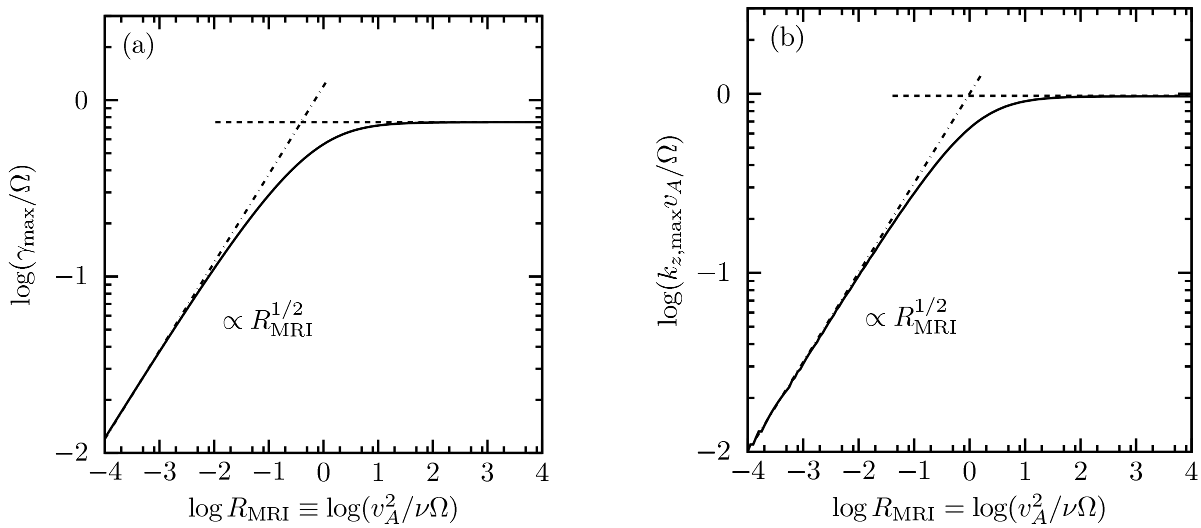

Fig. 2. Normalized maximum growth rate and the wavenumber of fastest growth as a function of the Reynolds number. The vertical and horizontal axes are logarithmic. Both quantities are proportional to $R_{\rm MRI}^{1/2}$ in the case with $R_{\rm MRI} \ll 1$.

The diffusion approximation can be used in the region with $\tau_{\rm tot} > 2/3$. In this region, the average mean-free-path of the neutrino is defined by $\langle\lambda\rangle = H/\tau_{\rm tot}$, and the neutrino viscosity $\nu \equiv 16\sigma_B T^4\langle\lambda\rangle/(15\rho c^2)$ is given by

$$\nu = 5\times 10^{12} T^2 \rho^{-2} \ \ {\rm cm}^2\ {\rm sec}^{-1}\,, \qquad (6)$$

(van den Horn & van Weert 1984). The spatial distributions of the neutrino depth and viscosity can be obtained in so far as the disk structure is determined.

2.2.2. *Simple Disk Model*

We adopt basic equations based on the Newtonian dynamics and construct the quasi-steady disk structure. Various disk models have been proposed as the central engine of GRBs, with detailed microphysics and/or general relativity in the framework of the α-prescription (Shakura & Sunyaev 1973; Popham et al. 1999; Di Matteo et al. 2002). For simplicity, we adopt a power-law model for the radial distribution of all physical quantities.

Assuming a power-law distribution with an index q, the surface density $\Sigma(r)$ is described as

$$\Sigma(r) = \Sigma_0 \hat{r}^{-q}\,, \qquad (7)$$

where $\hat{r} = r/r_s$ is the disk radius normalized by the Schwarzschild radius $r_s = 8.9\times 10^5 M_3$ cm ($M_3 = M_{\rm BH}/3M_\odot$ is a black hole mass normalized by 3 $M_\odot$). Σ_0 is a reference value of the surface density at $\hat{r} = 1$, and which is selected as $\Sigma_0 = 1.0\times 10^{18} f_\Sigma$ g cm^{-2}, with an arbitrary parameter f_Σ.

The disk temperature is assumed to have a power-law distribution with an index p,

$$T(r) = T_0 \hat{r}^{-p}\,, \qquad (8)$$

where T_0 is a reference value at $\hat{r} = 1$, and which is chosen as $T_0 = 4.3\times 10^{11} f_T$ K with an arbitrary parameter f_T (see also Masada et al. 2007b).

When the gas pressure dominates the other components, the sound speed $c_s = (k_B T/m_p)^{1/2}$ is

$$c_s = 6\times 10^9 f_T^{1/2} \hat{r}^{-p/2} \ \ {\rm cm\ sec}^{-1}\,. \qquad (9)$$

Ignoring the disk gravity, the hydrostatic equilibrium in the vertical direction determines the scale height of the disk $H = c_s/\Omega_K$,

$$H = 2\times 10^5 f_T^{1/2} M_3 \hat{r}^{-(p-3)/2} \ \ {\rm cm}\,, \qquad (10)$$

where the disk is assumed to rotate with the Keplerian velocity, $\Omega_K = 2\times 10^4 M_3^{-1}\hat{r}^{-3/2}{\rm sec}^{-1}$. The density structure $\rho = \Sigma/2H$ can be evaluated as

$$\rho = 2\times 10^{12} f_\Sigma f_T^{-1/2} M_3^{-1} \hat{r}^{(p-2q-3)/2} \ \ {\rm g\ cm}^{-3}\,. \qquad (11)$$

Using equations (8)-(11), the neutrino depth and viscosity are given by $\tau_{\rm tot} = 10^3 f_\Sigma f_T^2 \hat{r}^{-2p-q}$ and

$$\nu = 8\times 10^{10} f_\Sigma^{-2} f_T^3 M_3^{-1} \hat{r}^{3(1-p)+2q} \ \ {\rm cm}^2\ {\rm sec}^{-1}\,. \qquad (12)$$

The strength of the magnetic field is important for the MRI, although it is highly uncertain in the context of GRBs. We assume that the pre-collapse core of a massive star has a uniform poloidal field with strength $B \simeq 10^9$ G and average density $\rho_{\rm core} \simeq 2\times10^9$ g cm^{-3}. From flux conservation in the core-collapse phase, the radial structure of the poloidal field in the hyperaccretion disk is

$$B = 10^{11} f_\Sigma^{2/3} f_T^{-1/3} f_B M_3^{-2/3} \hat{r}^{(p-2q-3)/3} \quad {\rm G}\,, \quad (13)$$

where f_B is the arbitrary parameter for the field strength. The Alfvén speed then is

$$v_A = 2\times10^4 f_\Sigma^{1/6} f_T^{-1/12} f_B M_3^{-1/6} \hat{r}^{(p-2q-3)/12} {\rm cm\ s}^{-1}\,. \quad (14)$$

The power-law indices p and q are determined by the thermal equilibrium in the disk. There are two main cooling processes in the hyperaccretion disk, which are the advection and neutrino coolings. Considering that the advection cooling predominates, the indices are given by $p = 1.0$ and $q = 0.5$ (ADAF-type disk: Di Matteo et al. 2002). This is the case studied here.

2.3. *Evolution of MRI in Hyperaccretion Disk*

We evaluate the Reynolds number for the hyperaccretion disk. The radial profile of the Reynolds number is given, with equations (12) and (14), by

$$R_{\rm MRI} = 2\times10^{-7} f_\Sigma^{7/3} f_T^{-19/6} f_B^2 M_3^{5/3} \hat{r}^{(19p-14q-12)/6}\,. \quad (15)$$

For the ADAF-type disk with $f_\Sigma = f_T = 1$ (= fiducial model), the field parameter must be required to be $f_B \gtrsim 10^3$ for satisfying the condition (1). This indicates that a strong field of more than 10^{14}G is necessary for an efficient growth of the MRI in the hyperaccretion disk. When the magnetic field is weaker than this critical value, the inner region of the disk can be a "dead zone" where the MRI is suppressed by the neutrino viscosity.

For verifying this feature, the dispersion equation (2) is solved as a function of the disk radius. Figure 3 shows the maximum growth rate of the MRI for the cases with field parameters $f_B = 1$, 10, 10^2, and 10^3. The other arbitrary parameters are fixed to be unity ($f_\Sigma = f_T = 1$). The vertical and horizontal axes are normalized by the Keplerian velocity Ω_K and the Schwarzschild radius r_s. The critical radius dividing the neutrino-thick and thin regions is $r_{\rm crit} \simeq 20 r_s$. The part of this figure which is shaded in grey is the neutrino opaque region.

It is found that the maximum growth rate of the MRI in the neutrino-opaque region is much smaller than that in the transparent one in the case with $B \ll 10^{14}$ G. Turbulent motions at the nonlinear stage cannot be sustained when the growth rate of the MRI is much less than the angular velocity (Sano & Stone 2002). In contrast, the MRI-driven turbulence can actively grow in the neutrino-transparent region regardless of the field strength. In what follows, we construct a new evolutionary scenario for the hyperaccretion disk based on these new findings.

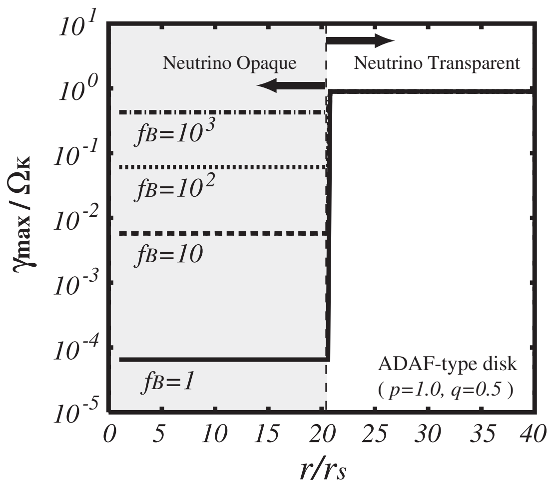

Fig. 3. The maximum growth rate of the MRI as a function of the disk radius for the cases with different field parameters $f_B = 1$, 10, 10^2, and 10^3. Other arbitrary parameters are fixed to be unity ($f_\Sigma = f_T = 1$). Gray shaded region is neutrino opaque one.

3. EPISODIC ACCRETION MODEL

In the weak field regime, the MRI is suppressed in the neutrino-opaque region (= the "dead zone"), but can actively grow in the neutrino-transparent region (= the active region). This feature has not been discussed in previous work. This can be an important physical clue to reveal the central engine of GRBs.

The existence of the dead zone can cause episodic disk accretion, which is the source of the short-term variability in the prompt emission of GRBs. We focus on the hyperaccretion disk formed with the "collapsar" scenario (Woosley 1993). In this scenario, the central $\sim 3\ M_\odot$ of a massive star collapses directly to a black hole, while infalling material forms an accretion disk with a mass of $\sim 1-2\ M_\odot$.

3.1. *Disk Evolution with Dead Zone*

We consider a dead zone with a size $r_{\rm crit} = 20 r_s$ formed in the inner part of a collapsar disk. Then, the angular momentum in the dead zone can be transported by the neutrino viscosity itself, not by the turbulent viscosity. The size of the neutrino viscosity can be represented by the α-prescription, $\alpha_\nu = \nu\Omega_K/c_s^2 \simeq 10^{-4}$ for the fiducial model. The mass accretion rate is thus given by

$$\dot{M}_{\rm out} = 4\pi r \rho H v_r \simeq 7 \times 10^{-4} \alpha_{\nu,-4} f_\Sigma f_T M_3 \dot{M}_\odot \,, \tag{16}$$

where $v_r = 3\nu/2r$ is the drift velocity. This is the matter extracted from the dead zone per unit time.

In the active region, the turbulent viscosity sustained by the MRI should dominate the angular momentum transport. Nonlinear studies tell us that the α-parameter of the MRI-driven turbulence would be $\alpha_t \sim 10^{-2}$ or less (Sano et al. 2004). Therefore, the mass inflow rate into the dead zone $\dot{M}_{\rm in}$ is

$$\dot{M}_{\rm in} \simeq 7 \times 10^{-2} \alpha_{t,-2} f_\Sigma f_T M_3 \dot{M}_\odot \,. \tag{17}$$

This is the mass of the baryonic matter which flows into the dead zone per unit time.

From equations (16) and (17), the baryonic matter is expected to be accumulated in the dead zone. The mass accumulation rate into the dead zone $\dot{M}_{\rm accu}$ is comparable to the inflow rate (i.e., $\dot{M}_{\rm in} \gg \dot{M}_{\rm out}$). If the mass accumulation with the rate $\dot{M}_{\rm accu}$ continues, at some stage the inner dead zone becomes gravitationally unstable. Then, the gravitational torque can cause intermittent mass accretion and drive discrete jets, which is thought to be the origin of short-term variability in the prompt emission of GRBs (Kobayashi et al. 1997).

The prospective evolutionary scenario of the hyperaccretion disk with a dead zone: the "Episodic Disk Accretion Model" is depicted schematically in Figure 4. In the next subsection, we discuss the typical evolutionary timescales and energetics of this model.

3.2. *Timescales and Energetics*

Considering the ADAF-type collapsar disk, the baryonic mass of the inner dead zone is

$$M_{\rm dz} = \int_{r_{\rm s}}^{r_{\rm crit}} 2\pi r \Sigma dr \simeq 0.2 f_\Sigma M_3^2 r_{\rm crit,20}^{3/2} M_\odot \,, \tag{18}$$

where $r_{\rm crit,20} = r_{\rm crit}/20 r_s$. Most of the matter is thus stored in the active region at early evolutionary stage. Since Toomre's Q value of the disk is

$$Q \equiv \Omega c_{\rm s}/(\pi G \Sigma) \simeq 8 f_\Sigma^{-1} f_T^{1/2} M_3^{-1} r_{\rm crit,20}^{-3/2} \,, \tag{19}$$

(Toomre 1964), the dead zone region is in the quiescent phase at the beginning. As time passes, the matter from the outer active region is accumulated near the critical radius. The gravitational instability begins to grow when the surface density at the critical radius becomes an order of magnitude larger than that of the initial quiescent phase (Figure 4*a*).

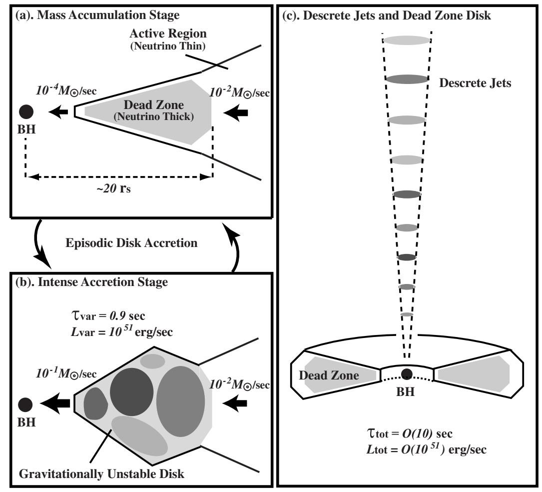

Fig. 4. Schematic picture of the Episodic Disk Accretion Scenario. Panel (a) shows the mass accumulation stage. Panel (b) represents the intense accretion stage. The dead zone alternates between these two stages and the explosive energy release occurs intermittently until the material of the outer active region is exhausted. Panel (c) is the final stage after the episodic accretion is terminated. Relativistic, multiple, discrete jets propagate outwards along the disk axis.

Once the outer edge of the dead zone becomes gravitationally unstable, spiral waves are exited globally in the dead zone, and which cause the intense mass accretion onto the black hole (Figure 4*b*). The mass accretion rate due to the gravitational torque can be described as

$$\dot{M}_{\rm g} \simeq 0.4 f_\Sigma f_{\rm T} M_3 \alpha_{g,05} \dot{M}_\odot \,, \tag{20}$$

where $\alpha_{g,05} = \alpha_g/0.05$ is the α-parameter of the gravitationally unstable disk normalized by its typical value (e.g., Lodato & Rice 2005). The duration of the intense accretion phase should be comparable to the viscous timescale of the dead zone;

$$\tau_{\rm g} = r^2/\nu \simeq 0.9 f_{\rm T}^{-1} M_3 \alpha_{g,05} r_{20}^{3/2} \ \ {\rm sec} \,. \tag{21}$$

The gravitational energy released during an intense accretion phase $E_{\rm g} \simeq \eta \dot{M}_{\rm g} \tau_{\rm g} c^2$ is

$$E_{\rm g} \simeq 2 \times 10^{53} f_\Sigma M_3^2 \alpha_{g,05}^2 r_{20}^{3/2} \eta_{0.4} \ {\rm erg} \,, \tag{22}$$

where $\eta_{0.4} = \eta/0.4$ is the normalized energy conversion efficiency from the rest-mass energy to the gravitational one for the Kerr black hole case.

After the intense mass accretion phase, the dead zone returns to the gravitationally stable state because the dead zone mass decreases. However the mass accretion from the active region continues constantly. The quiescent disk progressively evolves to the intense accretion phase again. This cycle is repeated and the explosive energy release occurs intermittently until the baryonic matter of the active region is exhausted. Finally the dead zone disk with a low mass accretion rate is left after the episodic accretion stage (Figure 4*c*).

If the episodic accretion is the origin of multiple relativistic shells, which cause the internal shocks (Kobayashi et al. 1997), the typical variable timescale $\tau_{\rm var}$ in the prompt emission should correspond to the duration of an intense accretion phase:

$$\tau_{\rm var} \simeq \tau_{\rm g} \simeq 0.9 \ \ {\rm sec}\,. \tag{23}$$

This can be the origin of observable log-normal feature in the short-term variability of the prompt emission (Shen & Song 2003). When a few percent of the gravitational energy is converted to the radiative one, the typical luminosity is evaluated as

$$L_{\rm var} \simeq f E_{\rm g}/\tau_{\rm var} \simeq 3\times 10^{51} f_{-2} \ \ {\rm erg\ sec}^{-1}\,, \tag{24}$$

where $f_{-2} = f/0.01$ is the conversion factor from the gravitational energy to the radiative one. These are almost identical to the observed timescale and peak luminosity of variable components of the prompt emission (Nakar & Piran 2002).

The episodic accretion is terminated when the material in the active region is exhausted. The total duration of the prompt emission is thus determined by the mass depletion time. Applying the mass inflow rate given by equation (17), the total duration and luminosity are evaluated as

$$\tau_{\rm tot} \simeq M_{\rm tot}/\dot{M}_{\rm in} \simeq \mathcal{O}(10) \ \ {\rm sec}\,, \tag{25}$$

$$L_{\rm tot} \simeq f\eta M_{\rm tot}c^2/\tau_{\rm tot} \simeq \mathcal{O}(10^{51}) \ \ {\rm erg\ sec}^{-1}\,, \tag{26}$$

where $M_{\rm tot}$ is the total mass of the accretion disk and is assumed to be $1-2\ M_\odot$. Our episodic accretion model of the collapsar disk can thus explain many observable features of GRBs qualitatively.

4. NONLINEAR ANALYSIS

4.1. *Numerical Setting*

Our evolutionary model is constructed in the framework of the linear analysis. It is necessary to study the nonlinear stage of the MRI in viscous media for establishing more concrete model. To reveal its nonlinear evolution, viscous MHD equations are solved with a finite-differencing code which was developed by Sano et al. (1998). Viscous terms are solved in the conservative form (Masada & Sano, in prep.). Using a local shearing box model (Hawley et al. 1995), basic equations are given by

$$\frac{\partial\rho}{\partial t} + \nabla\cdot(\rho v) = 0\,, \tag{27}$$

$$\frac{Dv}{Dt} = -\frac{\nabla P_{\rm eff}}{\rho} + \frac{(\mathbf{B}\cdot\nabla)\mathbf{B}}{4\pi\rho} - 2\Omega\times\mathbf{v} + 2q\Omega^2\mathbf{x} + \frac{\nabla\cdot\mathbf{S}}{\rho}\,, \tag{28}$$

$$\rho\frac{DE}{Dt} = -\nabla\cdot\left[P_{\rm eff}\mathbf{v} - \mathbf{S}\mathbf{v} - \frac{1}{4\pi}(\mathbf{v}\cdot\mathbf{B})\mathbf{B}\right]\,, \tag{29}$$

$$\frac{\partial\mathbf{B}}{\partial t} = \nabla\times(\mathbf{v}\times\mathbf{B})\,, \tag{30}$$

where

$$S_{ij} = \mu\left(\frac{\partial v_i}{\partial x_j} + \frac{\partial v_j}{\partial x_i}\right)\,,$$

$$P_{\rm eff} = P + \frac{|\mathbf{B}|^2}{8\pi} - \left(\chi - \frac{2}{3}\mu\right)(\nabla\cdot\mathbf{v})\,,$$

$$E = \frac{1}{2}|\mathbf{v}|^2 + e + \frac{|\mathbf{B}|^2}{2\rho}\,.$$

Assuming the ideal gas, the pressure is given by $P = (\gamma-1)\rho e$. In this simulation we assume that $\gamma = 5/3$ and the kinematic viscosity ν is spatially constant.

Unperturbed flow is assumed to be the Keplerian shear flow, then the velocity v_y is given by $v_y = -q\Omega x$. Since we focus on the local properties of the instability, we employ a numerical grid representing a small section of the disk interior for a local disk model. We assume that an initial magnetic field is a weak uniform field in the vertical direction.

A two-dimensional calculation is performed in the radial-vertical plane with a volume bounded by $x = z = \pm H$, where $H \equiv (2/\gamma)^{1/2}c_s/\Omega$ is the scale height of the disk. We use a uniform grid of 128^2 zones. A periodic boundary is used as the vertical boundary condition. For the radial one, we adopt a sheared periodic condition (Hawley et al. 1995). In this model, the vertical component of gravity is ignored. Thus, except for the shear velocity, the physical quantities are assumed to be spatially uniform; $\rho = \rho_0$ and $P = P_0$ where ρ_0 and P_0 are constant values. We choose normalizations with $\rho_0 = 1$, $H = 1$, $\Omega = 10^{-3}$, and $P_0 = 5\times 10^{-7}$ respectively.

4.2. *Results*

The system of the local disk model is characterized by the initial field strength $\beta_{\rm init} = 4\pi P/B_z^2$ and the Reynolds number $R_{\rm MRI}$ defined by equation (1). Here we show the results focusing on the effects of the Reynolds number. In what follows, we fix the initial field strength as $\beta_{\rm init} = 10000$.

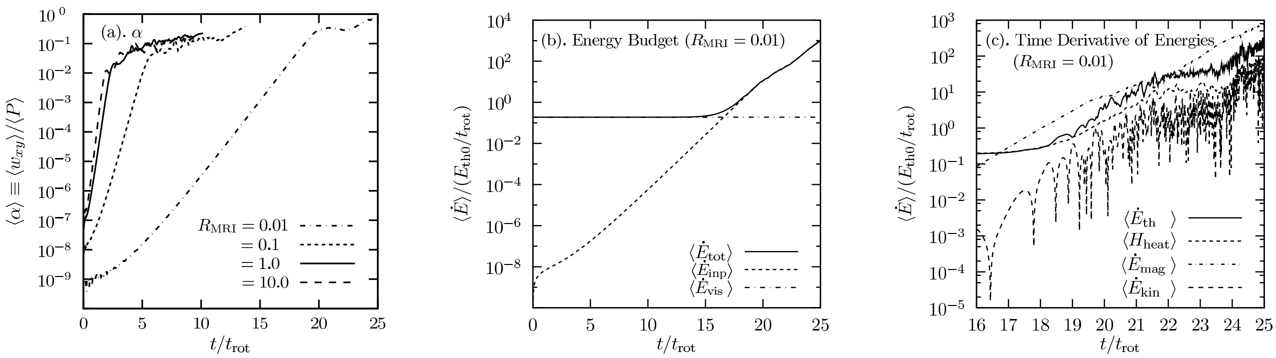

Fig. 5. Panel (a) shows the time evolution of the volume-averaged α parameter for the cases with different initial Reynolds numbers: $R_{\rm MRI} = 0.01$, 0.1, 1.0, and 10.0. The horizontal axis is the time normalized by $t_{rot} \equiv 2\pi/\Omega$. The time evolution of the volume-averaged time derivative of energy components is shown in Panels (b) and (c). The time-derivative of the total energy $\langle \dot{E}_{\rm tot}\rangle$, the energy input rate $\langle \dot{E}_{\rm inp}\rangle$, and the heating rate by the background shear motion $\langle \dot{E}_{\rm vis}\rangle$ are shown in Panel (b). The time derivatives of the thermal $\langle \dot{E}_{\rm th}\rangle$ and magnetic energies $\langle \dot{E}_{\rm mag}\rangle$, and the viscous heating rate by the turbulent motion $\langle \dot{E}_{\rm vis}\rangle$ are shown in Panel (c).

We find that the channel solution appears for all models in spite of the size of the Reynolds number. This channel flow continues growing and is not saturated even with the viscous dissipation process. The viscous dissipation cannot damp the MHD turbulence in the nonlinear regime. This feature of the MRI is quite different with the case considering magnetic resistivity (Sano et al. 1998). In resistive media, the channel solution is appeared for the models with larger Lundquist numbers $S_{\rm MRI} \gtrsim 1$. However, the MHD turbulence is damped when $S_{\rm MRI} \lesssim 1$.

The time evolution of the volume-averaged $\alpha = \langle w_{xy}\rangle/\langle P\rangle$ is depicted in Figure 5a for the cases with $R_{\rm MRI} = 0.01$, 0.1, 1.0, and 10.0, where w_{xy} is the $x - y$ component of the stress tensor defined by

$$\langle w_{xy}\rangle = -\langle B_x B_y\rangle/4\pi + \langle \rho v_x \delta v_y\rangle\,. \qquad (31)$$

Note that the horizontal axis is the time in the unit of the disk rotation $t_{\rm rot} \equiv 2\pi/\Omega$. The MRI can not saturate even in the low Reynolds number regime.

Using the viscous MHD equations, the time derivative of the volume-averaged total energy within the shearing box $\langle \dot{E}_{\rm tot}\rangle$ can be obtained as

$$\langle \dot{E}_{\rm tot}\rangle \simeq \langle \dot{E}_{\rm inp}\rangle + \langle \dot{E}_{\rm vis}\rangle\,, \qquad (32)$$

where $\langle \dot{E}_{\rm inp}\rangle \equiv q\Omega\langle w_{xy}\rangle$ is the energy input rate through the sheared periodic boundary, and $\langle \dot{E}_{\rm vis}\rangle \simeq \nu q^2\Omega^2\langle\rho\rangle$ is the viscous heating rate by the background shear motion. (see Masada & Sano in prep.). This relation is clearly demonstrated in Figure 5b. The time evolution of $\langle \dot{E}_{\rm tot}\rangle$, $\langle \dot{E}_{\rm inp}\rangle$ and $\langle \dot{E}_{\rm vis}\rangle$ are shown for the case $R_{\rm MRI} = 0.01$ here. This indicates that our calculations perfectly explain the energy budget of the system.

Figure 5c depicts the time evolution of the time derivative of various energy components $\langle \dot{E}_{\rm th}\rangle$, $\langle \dot{E}_{\rm m}\rangle$, $\langle \dot{E}_{\rm k}\rangle$ and $\langle H\rangle$ for the case $R_{\rm MRI} = 0.01$. Here the viscous heating rate $\langle H\rangle$ is defined by

$$\langle H\rangle \equiv \xi(\nabla\cdot v)^2 + \frac{\mu}{2}\left(\frac{\partial v_i}{\partial x_j} + \frac{\partial v_j}{\partial x_i}\right)^2\,, \qquad (33)$$

where $\xi \equiv \chi - 2\mu/3$. We find that the increasing rate of the thermal energy $\langle \dot{E}_{\rm th}\rangle$ is much larger than the viscous heating rate by the turbulent motion $\langle H\rangle$. This means that the systematic, numerical resistivity takes a major role in the heating of the system rather than the kinematic viscosity. This might be the important clue for revealing the cause of the saturation of the MRI in the doubly diffusive media with the resistivity and viscosity (see also Lesur & Longaretti 2007; Fromang et al. 2007).

4.3. *Discussion*

4.3.1. *Viscosity versus Resistivity*

We discuss the physical reason why the MRI is not saturated and the channel flow continues growing in highly viscous media. Despite the size of the Reynolds number, in the viscous media, the lower limit for the unstable wavelength of the MRI is given by $\lambda_{\rm crit} \simeq v_A/\Omega$ (see Figure 1). At the early linear phase, the radial and azimuthal components of the magnetic field continue to grow exponentially. The lower limit for the unstable wavelength in the radial direction then becomes longer as the instability grows. The radial wavenumber of unstable modes thus approaches $k_r \to 0$, while the vertical component of the magnetic field does not grow exponentially as in the linear mode. The wavevectors of the

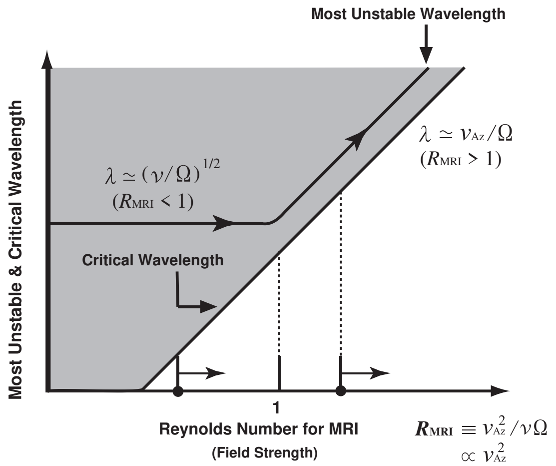

Fig. 6. Illustration of the characteristic wavelength of the MRI as a function of $R_{\rm MRI}$. Shaded area denotes the unstable region expected by the linear analysis. Assuming a uniform and constant diffusivity ν, $R_{\rm MRI}$ is proportional to the squared Alfvén speed. The characteristic value of $R_{\rm MRI}$ increases as the instability grows. In spite of the initial size of $R_{\rm MRI}$, the characteristic scale becomes longer as the magnetic field grows, so that the system evolves to a less dissipative one and is not saturated.

unstable modes become parallel to the vertical axis. They could be the exact solution of the MHD equations even in the nonlinear regime (Goodman & Xu 1994). As the strength of the magnetic field grows, the characteristic unstable scale shifts to larger values, for which the viscous dissipation is less effective. The channel solution thus continues growing even when the dissipation process is included (see Figure 6).

In contrast, the lower limit for the unstable wavelength is expressed approximately by $\lambda_{\rm crit} \sim \eta/v_A$ in resistive media (Sano & Miyama 1999). When the magnetic field is amplified by the MRI, the lower limit for the unstable wavelength shifts to lower values. Therefore, in the nonlinear stage, many modes with wavelength larger than η/v_A are unstable. These modes are not exponentially growing solutions because their wavevectors are not parallel. Otherwise, they enhance the ohmic dissipation in the turbulent state. The MRI can thus saturate in highly resistive media (see Fig. 4 in Sano et al. 1998).

4.3.2. *Comment on Episodic Disk Accretion Model*

Finally we comment on our "Episodic Disk Accretion Model", based on the results of the nonlinear analysis. As is described in the previous subsection, even in low Reynolds number media $R_{\rm MRI} \ll 1$, the angular momentum can be transported efficiently at the nonlinear stage. This is contrary to the assumption used in our new model (i.e., that the turbulent motion is damped at the nonlinear stage). However, the linear evolutionary phase is maintained for a long time and the turbulent viscosity remains small during this phase. For instance, in the case with $R_{\rm MRI} = 10^{-3}$, it takes $\sim 100t_{\rm rot}$ for the MRI to reach the nonlinear stage and then α remains small compared to the size of the neutrino viscosity itself $\alpha_\nu \simeq 10^{-4}$. We thus consider that our new evolutionary model can be promising when the field strength is much weaker than the critical value $B_{\rm crit} = (4\pi\rho\nu\Omega)^{1/2}$. For revealing the physical picture of the central engine of GRBs, multi-dimensional local and global simulations of the MRI must be performed in the context of the hyperaccretion disk. This is our future work.

REFERENCES

Balbus, S. A., & Hawley, J. F. 1991, ApJ, 376, 214
Di Matteo, T., Perna, R., & Narayan, R. 2002, ApJ, 579, 706
Fromang, S., Papaloizou, J., Lesur, G., & Heinemann, T. 2007, A&A, 476, 1123
Goodman, J., & Xu, G. 1994, ApJ, 432, 213
Hawley, J. F., Gammie, C. F., & Balbus, S. A. 1995, ApJ, 440, 742
Kobayashi, S., Piran, T., & Sari, R. 1997, ApJ, 490, 92
Lee, W. H., Ramirez-Ruiz, E., & Page, D. 2005, ApJ, 632, 421
Lesur, G., & Longaretti, P.-Y. 2007, MNRAS, 378, 1471
Lodato, G., & Rice, W. K. M. 2005, MNRAS, 358, 1489
Masada, Y., Sano, T., & Shibata, K. 2007a, ApJ, 655, 447 (MSS07)
Masada, Y., Kawanaka, N., Sano, T., & Shibata, K. 2007b, ApJ, 663, 437
Nakar, E., & Piran, T. 2002, MNRAS, 331, 40
Narayan, R., Paczynski, B., & Piran, T. 1992, ApJ, 395, L83
Popham, R., Woosley, S. E., & Fryer, C. 1999, ApJ, 518, 356
Sano, T., Inutsuka, S., & Miyama, S. M. 1998, ApJ, 506, L57
Sano, T., & Miyama, S. M. 1999, ApJ, 515, 776
Sano, T., & Stone,J. M. 2002, ApJ, 577, 534
Sano, T., Inutsuka, S., Turner, N. J., & Stone, J. M. 2004, ApJ, 605, 321
Shakura, N. I., & Sunyaev, R. A. 1973, A&A, 24, 337
Shapiro, S. L., & Teukolsky, S. A. 1983, Black Holes, White Dwarfs, and Neutron Stars: The Physics of Compact Objects (New York: Wiley Interscience), 549
Shen, R.-F., & Song, L.-M. 2003, PASJ, 55, 345
Toomre, A. 1964, ApJ, 139, 1217
van den Horn, L. J., & van Weert, C. G. 1984, A&A, 136, 74
Woosley, S. E. 1993, ApJ, 405, 273